



CHORUS

This is the accepted manuscript made available via CHORUS. The article has been published as:

Ideal strength and structural instability of aluminum at finite temperatures

Wei Zhou, Yi Zhang, Hong Sun, and Changfeng Chen

Phys. Rev. B **86**, 054118 — Published 24 August 2012

DOI: [10.1103/PhysRevB.86.054118](https://doi.org/10.1103/PhysRevB.86.054118)

Ideal Strength and Structural Instability of Aluminum at Finite Temperatures

Wei Zhou,^{1,2} Yi Zhang,² Hong Sun,^{1,2,*} and Changfeng Chen^{2,†}

*¹Department of Physics, Shanghai Jiao Tong University,
Shanghai 200240, and Key Laboratory of Artificial Structures
and Quantum Control, Ministry of Education, China*

*²Department of Physics and High Pressure Science and Engineering Center,
University of Nevada, Las Vegas, Nevada 89154, USA*

Abstract

We have calculated the ideal strength of aluminum at finite temperatures by implementing an *ab initio* molecular dynamics (AIMD) method that treats elastic instability, dynamic instability and thermodynamics in a unified first-principles approach. The results reveal significant changes in fundamental mechanical properties of aluminum: (i) the ideal strength drops precipitously with increasing temperature, by as much as 60% at room temperature compared to $T=0$ K; (ii) the structural instability modes change qualitatively from dynamic phonon softening at low temperature to elastic failure at high temperature; (iii) the highly anisotropic low-temperature tensile strength becomes considerably more isotropic with rising temperature. Phonon calculations predict the disappearance of soft phonon modes near room temperature due to phonon anharmonic interactions, in excellent agreement with the AIMD results. This work sets key benchmarks for aluminum and opens a new avenue for studying material deformation and strength at finite temperatures.

PACS numbers: 62.20.-x, 81.40.Jj, 61.50.Ah, 63.20.-e

Accurate prediction and analysis of the stability of crystal lattices is fundamentally important in materials science; it holds the key to understanding the mechanism for material deformation and strength. Recent developments in computational physics have enabled first-principles calculations of peak stresses (i.e., ideal strengths) in the stress-strain relations of a crystal lattice along specific deformation paths and the structural deformation modes leading to elastic instabilities¹⁻¹¹. Meanwhile, dynamic instability of a crystal lattice has been studied via *separate* calculations of the phonon spectra of the crystal lattice at each step along every deformation pathway. The appearance of imaginary frequencies in the phonon spectra indicates the beginning of the dynamic instability of the crystal lattice¹²⁻¹⁵. These calculations, however, are all performed at T=0 K, thus ignoring thermodynamic effects that are expected to alter material behavior at high temperatures. It is highly desirable to develop a method that can treat different lattice instabilities and thermodynamics in a unified first-principles approach.

Here we explore the finite-temperature mechanical behavior of aluminum (Al), which is one of the most widely used metals owing to its unique properties of light weight, high corrosion resistance, good electric and thermal conductivities, and large plasticity. Despite numerous past studies^{1,3,8,9,12,16-25}, there remain questions on the fundamental properties of Al, such as how the temperature would affect the strength under various loading conditions and whether the lattice instability behaviors predicted at T=0 K would change with rising temperature. Previous first-principles calculations (at T=0 K) predict that under the $\langle 001 \rangle$, $\langle 011 \rangle$, $\langle 111 \rangle$ uniaxial tension and the $\{111\} \langle 112 \rangle$ shear deformation, dynamic phonon instabilities always precede the elastic instabilities determined by the peak stresses in ideal strength calculations¹². More interestingly, all the unstable phonon modes in Al at T=0 K are shear in nature, which suggests that inhomogeneous shear failure may be an intrinsic property of Al under plastic deformations¹². The effect of temperature on the properties of Al has been examined by several molecular dynamics (MD) calculations with various empirical potentials^{20-22,25}. However, the complex electron distribution and directional bonding in Al^{3,23} make it difficult to construct an empirical potential that can accurately describe the bond distortion or rebonding at large plastic deformations in all crystallographic directions. Consequently, the stress-strain relations of Al generated by empirical MD (at T=0 K) cannot reproduce the results by first-principles methods in the peak stresses and/or the critical strains where the peak stresses appear^{3,8,12,21,25}. This situation underscores the urgent need

for a first-principles approach that can set key benchmarks on fundamental mechanical properties of Al at finite temperatures and, in a broader sense, provide a reliable method for studying the temperature effect on the behavior and mechanism of material deformation and strength.

In this paper, we report on a study of the ideal strength and lattice instability of Al at finite temperatures by implementing an *ab initio* molecular dynamics (AIMD) method, in which the forces among atoms are calculated directly at every MD step from the electronic structure of the deformed Al lattice from first principles. The AIMD incorporates the thermodynamic motions of atoms in the ideal strength calculations and treats the ideal strength (elastic instability) and phonon softening (dynamic instability) in one unified calculation. The structural failure modes of Al at different temperatures obtained from AIMD are then compared with the phonon spectra of the deformed Al lattice calculated at finite temperatures. Our calculations reveal a qualitative change of mechanism for lattice instability in Al in that under the $\langle 001 \rangle$, $\langle 011 \rangle$, $\langle 111 \rangle$ uniaxial tension and the $\{111\} \langle 112 \rangle$ shear deformation, the dynamically unstable phonon modes at $T=0$ K¹² disappear at room or higher temperature, due to phonon anharmonic interactions in Al, and the elastic instability determined by the peak stresses becomes dominant. The temperature also has sensitive effects on the reduction of both the magnitude and directional (anisotropic) nature of the ideal strength of Al compared to its $T=0$ K results¹².

The stress-strain relations of Al at finite temperatures under tensile and shear deformations are calculated using the AIMD package of the VASP code²⁶, in which the temperature dependent total free energy of the electron subsystem is directly minimized at each AIMD step; the gradient of the total free energy gives the forces (the Hellmann-Feynman forces at finite temperatures) that dictate the motion of the atoms which are coupled to a Nosé thermostat (canonical ensemble) to maintain a constant temperature of the system²⁷. A cubic supercell with 32 Al atoms and a $7 \times 7 \times 7$ Monkhorst-Pack (MP) k-point grid are used in the AIMD calculations²⁸, adopting the projector augmented-wave potentials (PAW)²⁹ and the Wang-Perdew generalized gradient approximation (GGA) exchange-correlation functional³⁰ with a 140 eV energy cutoff (higher energy cutoffs tested up to 250 eV produce stress variations of less than 0.1 GPa). The quasistatic stress-strain relations of Al along various deformation paths at a constant temperature are determined using a method similar to the one described previously¹. The lattice vectors of the Al supercell are incrementally deformed

in the direction of the applied strain. At each deformation step the structure is relaxed such that all the AIMD average residual components of the Hellmann-Feynman stress tensor orthogonal to the applied strain and the average force on each atom are less than 0.1 GPa and 0.01 eV/Å, respectively, while keeping the applied strain fixed. The shape of and the average atomic positions in the supercell are determined by the (constrained) atomic relaxations. The AIMD average at each deformation step is performed by the integration of the equations of motion of the atoms in the deformed Al lattice with a time step of 2 fs and 2000 AIMD steps where the initial atomic positions at each step are determined by the AIMD average atomic positions of the previous deformation step. The last 1500 steps are used to calculate the average stresses and atomic positions. The average stress-strain relations and atomic motions of the Al lattice under the $\langle 001 \rangle$, $\langle 011 \rangle$, $\langle 111 \rangle$ uniaxial tension and the $\{111\} \langle 112 \rangle$ shear deformations are determined at different temperatures. The AIMD testing runs for the equilibrium structures of Al at different temperatures give a thermal expansion coefficient of 23.5 (in unit of $10^{-6}/\text{K}$) at $T=300$ K, in good agreement with the experimental result 23.6.³¹ We also calculated the phonon spectra of the Al lattice at specific deformation strains and different temperatures using the SCAILD code³², which includes phonon anharmonic interactions in the calculation that makes the phonon frequencies temperature-dependent, with a $5 \times 5 \times 5$ supercell of 125 atoms and $4 \times 4 \times 4$ MP k-point grid. The phonon frequencies with wave vectors commensurate with the supercell and the forces induced by the atomic displacements of these phonon modes, which are used to determine the new phonon frequencies, are calculated using the VASP code, adopting the same PAW potential and GGA functional as those in the AIMD calculations. At least 40 iterations between the phonon frequencies and induced forces are needed to obtain the converged phonon frequencies that include the anharmonic interactions of the Al lattice vibrations at room or higher temperatures³³.

In Fig. 1, we plot the AIMD calculated average stress-strain relations of Al under various tensile and shear deformation directions at different temperatures. The AIMD stress-strain curves at $T=0$ K agree well with previous first-principles results¹². Drastic reductions in the peak stresses and the corresponding critical strains occur in the tensile $\langle 001 \rangle$ and $\langle 111 \rangle$ directions at room or higher temperatures. The ratio of the peak stresses under the $\langle 001 \rangle$, $\langle 011 \rangle$ and $\langle 111 \rangle$ tensions at $T=0$, 300 and 700 K are 11.5/4.2/10.0, 4.7/3.2/5.2 and 2.3/2.1/3.5, respectively. It is surprising that even at room temperature, the tensile

strengths have reduced by about 60%, 24%, and 48%, respectively, in these three directions compared to the $T=0$ K results. Increasing temperature also leads to a drastic reduction in the large stress anisotropy in the tensile strengths of Al at $T=0$ K¹². Perhaps the most intriguing result unveiled by our AIMD calculations is the qualitative change in the structural instability modes of Al as temperature rises: at $T=0$ K, phonon instabilities happen before the stress peaks under both the tensile and shear deformation¹²; at high temperatures (at or above room temperature), however, the stress peaks much sooner, which precedes the phonon instabilities and, as we will show, the elastic instabilities become the dominant mechanism for structural failure of Al at or above room temperature.

Two distinct types of stress-strain curves are observed at finite temperatures (see Fig. 1): one with a sharp drop in stress past the peak stress (see the tensile $\langle 001 \rangle$ curves at $T=100$ and 300 K) and the other with a gradual decrease in stress past the peak (all the remaining curves in Fig. 1 at $T \neq 0$ K). They correspond to different failure modes of lattice instabilities under structural deformation. In Fig. 2(a), we plot the AIMD calculated motion trajectory (solid curves) of atoms in Al under the tensile $[001]$ deformation in the $S_1, S_2 \dots$ layers [defined in Fig. 2(b)] perpendicular to the $[001]$ direction at $T=300$ K. When the $[001]$ tensile strain is at $\epsilon \leq 0.14$ before the drop of stress, the tension only causes a slight reduction of the lattice constants in the (001) plane (the Poisson effect). As the $[001]$ tensile strain reaches $\epsilon=0.15$ (at $T=300$ K), which is slightly smaller than the critical strain ($\epsilon=0.155$) where the phonon instability occurs at $T=0$ K (see Fig. 1), a (inhomogeneous) structural transformation of shear character in the (001) plane sets in and transforms the “square” lattices in the $S_1, S_2 \dots$ layers into “hexagonal” ones. The average shifts of atomic positions relative to their positions prior to the structural transformation are consistent with the eigen-vectors of the unstable phonon mode under the $[001]$ tensile deformation predicted at $T=0$ K¹². It shows that the unified AIMD approach for ideal strength calculations at finite temperatures can indeed capture the unstable phonon induced dynamic lattice instability. The final structure of Al under the $[001]$ tensile strain at $T=300$ K after this shear-type structural transformation at $\epsilon = 0.15$ is a close-packed stacking of the “hexagonal” layers. For the $2 \times 2 \times 2$ cubic supercell, we obtain an $ABCBA \dots$ stacking structure. However, this stacking is the result of an artificial constraint in the $2 \times 2 \times 2$ cubic supercell that requires that the atomic motions in the S_1 and S_5 layers be identical due to the periodic condition imposed by the supercell [see Fig. 2(b)]. To avoid any AA stacking of the hexagonal

layers which increases the total energy, the low energy structure consistent with the $2 \times 2 \times 2$ cubic supercell is the $ABCBA \cdots$ stacking structure. We performed the same tensile $[001]$ calculation at $T=300$ K using a $2 \times 2 \times 6$ cubic supercell, which is commensurate with both the $ABCBA \cdots$ and $ABCABC \cdots$ stacking. We obtained the same stress peak and the critical strain at which the shear-type structural transformation happens, which shows that the $2 \times 2 \times 2$ supercell can adequately describe the ideal strength and deformation mode in Al; but the final structure after the transformation at $\epsilon = 0.15$ has the $ABCABC \cdots$ stacking, which is the structure of the equilibrium Al structure in the $[111]$ direction. The calculated atomic inter-layer distance of Al in the $[001]$ direction at the $[001]$ tensile strain $\epsilon = 0.15$ ($T=300$ K) is 2.365 \AA , which is close to the calculated atomic inter-layer distance (2.352 \AA) of Al in the $[111]$ direction at the equilibrium structure ($T=300$ K). So the shear-type structural transformation under the $[001]$ tensile strain at $\epsilon = 0.15$ ($T=300$ K) transforms the highly stressed Al structure in the $[001]$ direction into the equilibrium Al structure in the $[111]$ direction, which has the lowest total energy, and releases all the stress in the lattice. In Fig. 2(d), we plot the calculated AIMD average atom positions in the S_1, \cdots, S_4 layers for the $2 \times 2 \times 6$ cubic-supercell at $T=300$ K and under the $[001]$ tensile strain at $\epsilon = 0.15$. The results show a good hexagonal lattice with an $ABCABC \cdots$ stacking.

In Fig. 3(a), we plot the AIMD calculated motion trajectory (solid curves) of atoms in Al under the tensile $[101]$ deformation in the $S_1, S_2 \cdots$ layers [defined in Fig. 3(b)] perpendicular to the $[101]$ tensile direction at $T=300$ K with the strain $\epsilon=0$ (at the equilibrium), $\epsilon=0.1$ (at the stress peak) and $\epsilon=0.12$ (after the stress peak). Apart from the tensile stretching in the $[101]$ direction, no shear-type structural transformation is found even at $\epsilon = 0.12$, which is far beyond the critical strain ($\epsilon = 0.095$) at which the unstable phonon modes corresponding to a (inhomogeneous) shear sliding in the $(111)[\bar{1}1\bar{2}]$ direction is predicted at $T=0$ K¹² (see also Fig. 1). We also tested our results by increasing the AIMD steps from 2000 to 10000 at $\epsilon = 0.1$ and 0.12 . The obtained average stresses and atomic positions are almost identical, which indicates the convergence of our calculations with the number of the AIMD steps. Similarly, no (inhomogeneous) shear-type structural transformation is found for the $[001]$ tensile deformation at $T=500$ and 700 K, the tensile $[101]$ deformation at $T=700$ K, the $[111]$ tensile deformation at $T=300$ and 700 K, and the $(111)[\bar{1}1\bar{2}]$ shear deformation at $T=300$ and 700 K at the strains near their peak stresses, while the $T=0$ K calculations¹² predict such (inhomogeneous) shear-type unstable phonon modes in all these deformations

before the stress peaks are reached (see also Fig. 1).

To understand the disappearance of the unstable phonon modes which give rise to the dynamic shear instabilities at $T=0$ K for Al under tensile and shear deformations¹², we calculate the phonon spectra of Al under the $\langle 001 \rangle$, $\langle 011 \rangle$, $\langle 111 \rangle$ uniaxial tension and the $\{111\} \langle 112 \rangle$ shear deformations at $T=0$ K with the harmonic approximation at each deformation step and the phonon spectra of Al including the phonon anharmonic interactions at high temperatures deformed along the various tensile and shear directions at the strains after imaginary phonon frequencies appear at $T=0$ K. Our $T=0$ K calculations determine the onset of the phonon instability as shown in Fig. 1, and the obtained phonon spectra (not shown here) agree well with those of the previous calculations¹². In Fig. 4, we compare the calculated phonon spectra of Al at temperatures $T=0$ (harmonic approximation), 300 and 700 K under the $\langle 001 \rangle$, $\langle 011 \rangle$, $\langle 111 \rangle$ uniaxial tension and the $\{111\} \langle 112 \rangle$ shear deformations at the strains after imaginary phonon frequencies appear at $T=0$ K. The results show clearly that, except for the tensile $[001]$ deformation, all the unstable phonon modes found at $T=0$ K stabilize due to the phonon anharmonic interactions near room temperature. Even for the $[001]$ tensile, the unstable phonon mode disappears above room temperature. These results agree well with our AIMD results presented above in that the (inhomogeneous) shear-type structural transformations related to the unstable phonon modes exist in Al at the room temperature only in the $[001]$ tensile deformation, while in other deformation directions the unstable phonon modes all disappear. At higher temperatures, all the unstable phonon modes in Al stabilize, and the structural failure modes of Al are dominated by the elastic instabilities.

In summary, we have implemented AIMD simulations to determine the ideal strength and structural instability modes of Al at finite temperatures. The dynamic phonon instabilities under the $\langle 001 \rangle$, $\langle 011 \rangle$, $\langle 111 \rangle$ uniaxial tension and the $\{111\} \langle 112 \rangle$ shear deformations predicted at $T=0$ K disappear at or above room temperature, and the elastic instabilities determined by the peak stresses become the dominate failure modes. Rising temperature also induces significant reduction in the magnitude of the ideal strength and makes the tensile strength of Al much more isotropic. We also have performed phonon calculations and found that the phonon anharmonic interactions stabilize the low-temperature dynamic phonon instabilities near or above room temperature, which agrees with the AIMD calculations. These results set key benchmarks for fundamental mechanical properties of Al at

finite temperatures. Though in practice the strengths of crystalline materials are controlled by many effects, such as defects and diffusion processes, the ideal strength calculations predict the crystal incipient plasticity.¹⁷ The present work advances computational materials research by opening a new avenue for determining the ideal strength and lattice instability at finite temperatures in a unified first-principles approach.

This work was supported by DOE Grant No. DE-FC52-06NA26274 at UNLV and NNSF of China Grant No. 11174200 at SJTU. H. Sun also appreciates the support of the Science and Engineering Interdisciplinary Research Foundation of SJTU.

* Corresponding author; Email:hsun@sjtu.edu.cn

† Corresponding author; Email:chen@physics.unlv.edu

- ¹ D. Roundy, C. R. Krenn, M. L. Cohen, and J. W. Morris Jr., Phys. Rev. Lett. **82**, 2713 (1999).
- ² S. H. Jhi, S. G. Louie, M. L. Cohen, and J. W. Morris Jr., Phys. Rev. Lett. **87** 075503 (2001).
- ³ S. Ogata, J. Li, and S. Yip, Science **298** 807 (2002).
- ⁴ X. Blase, P. Gillet, A. S. Miguel, and P. Melinon, Phys. Rev. Lett. **92** 215505 (2004).
- ⁵ Y. Zhang, H. Sun, and C. F. Chen, Phys. Rev. Lett. **93**, 195504 (2004); **94** 145505 (2005).
- ⁶ M. G. Fyta, I. N. Remediakis, P. C. Kelires, and D. A. Papaconstantopoulos, Phys. Rev. Lett. **96** 185503 (2006).
- ⁷ J. Yang, H. Sun, and C. F. Chen, J. Am. Chem. Soc. **130** 7200 (2008).
- ⁸ M. Jahnátek, J. Hafner, and M. Krajčí, Phys. Rev. B **79** 224103 (2009).
- ⁹ S. Ogata, Y. Umeno, and M. Kohyama, Modelling Simul. Mater. Sci. Eng., **17** 013001 (2009).
- ¹⁰ Z. C. Pan, H. Sun, Y. Zhang, and C. F. Chen, Phys. Rev. Lett. **102** 055503 (2009).
- ¹¹ W. Zhou, H. Sun, and C. F. Chen, Phys. Rev. Lett. **105** 215503 (2010).
- ¹² D. M. Clatterbuck, C. R. Krenn, M. L. Cohen, and J. W. Morris Jr., Phys. Rev. Lett. **91** 135501 (2003).
- ¹³ S. M. -M. Dubois, G. -M. Rignanese, T. Pardoen, and J. -C. Charlier, Phys. Rev. B **74** 235203 (2006).
- ¹⁴ F. Liu, P. B. Ming, and J. Li, Phys. Rev. B **76** 064120 (2007).
- ¹⁵ C. A. Marianetti and H. G. Yevick, Phys. Rev. Lett. **105** 245502 (2010).

- ¹⁶ F. Milstein and S. Chantasiriwan, Phys. Rev. B **58** 6006 (1998).
- ¹⁷ J. Li, K. J. Van Vliet, T. Zhu, S. Yip, and S. Suresh, Nature **418** 307 (2002).
- ¹⁸ V. Tomar and M. Zhou, Phys. Rev. B **73** 174116 (2006).
- ¹⁹ A. M. Minor, S. A. Syed Asif, Z. W. Shan, E. A. Stach, E. Cyrankowski, T. J. Wyrobek, and O. Warren, Nat. Mater. **5** 697 (2006).
- ²⁰ S. D. Chen, F. J. Ke, M. Zhou, and Y. L. Bai, Acta Mater. **55** 3169 (2007).
- ²¹ R. D. Nyilas and R. Spolenak, Acta Mater. **56** 5627 (2008).
- ²² M. Hou and O. Melikhova, Acta Mater. **57** 453 (2009).
- ²³ P. N. H. Nakashima, A. E. Smith, J. Etheridge, and B. C. Muddle, Science **331** 1583 (2011).
- ²⁴ L. Pastor-Abia, M. J. Caturla, E. SanFabian, G. Chiappe, and E. Louis, Phys. Rev. B **83** 165441 (2011).
- ²⁵ A. M. Iskandarov, S. V. Dmitriev, and Y. Umeno, Phys. Rev. B **84** 224118 (2011).
- ²⁶ <http://www.vasp.at/>
- ²⁷ G. Kresse and J. Hafner, Phys. Rev. B **49** 14251 (1994).
- ²⁸ H. J. Monkhorst and J. D. Pack, Phys. Rev. B **13** 5188 (1976).
- ²⁹ P. E. Blöchl, Phys. Rev. B **50** 17953 (1994); G. Kresse and D. Joubert, Phys. Rev. B **59** 1758 (1999).
- ³⁰ J. P. Perdew, J. A. Chevary, S. H. Vosko, K. A. Jackson, M. R. Pederson, D. J. Singh, and C. Fiolhais, Phys. Rev. B **46** 6671 (1992)
- ³¹ N. W. Ashcroft and N. D. Mermin, *Solid State Physics* (Thompson Learning, Inc., London, 1976), p.496.
- ³² http://web.mac.com/petros.souvatzis/Webbplats_2/SCAILD.html
- ³³ P. Souvatzis, O. Eriksson, M. I. Katsnelson, and S. P. Rudin, Phys. Rev. Lett. **100** 095901 (2008).

Figure Captions

Fig. 1 (Color online) The AIMD calculated average stress-strain relations of Al in a cubic supercell with 32 Al atoms under various tensile and shear deformation directions at different temperatures. The (red) solid circles indicate the phonon instability (PI) determined at T=0 K, which begins at the strains equal to 0.155, 0.095, 0.145 and 0.145, respectively, for the $\langle 001 \rangle$, $\langle 011 \rangle$, $\langle 111 \rangle$ uniaxial tension and the $\{111\} \langle 112 \rangle$ shear deformation.

Fig. 2 (Color online) (a) The calculated AIMD motion trajectory (solid lines) of atoms in an Al $2 \times 2 \times 2$ cubic-supercell at T=300 K under the $[001]$ tensile strains $\epsilon=0$ (at the equilibrium), $\epsilon=0.14$ (before the stress drop) and $\epsilon=0.15$ (just after the stress drop) in the atomic layers S_1, S_2, \dots perpendicular to the $[001]$ tensile direction. The (blue) squares and (red) circles indicate the initial and AIMD average atomic positions at each strain deformation step. For clarity, the atomic displacements relative to the average positions are enlarged by a factor of 3 and 2 for $\epsilon = 0$ and 0.14, respectively. (b) A $1 \times 1 \times 2$ cubic-supercell of Al that defines the S_1, S_2, \dots atomic layers perpendicular to the $[001]$ tensile direction. (c) The enlarged motion trajectory of an Al atom in the S_2 layer. (d) The calculated AIMD average atomic positions in the S_1, \dots, S_4 layers for a $2 \times 2 \times 6$ cubic-supercell at T=300 K and under the $[001]$ tensile strain at $\epsilon = 0.15$.

Fig. 3 (Color online) (a) The calculated AIMD motion trajectory (solid lines) of atoms in an Al $2 \times 2 \times 2$ cubic-supercell at T=300 K under the $[101]$ tensile strains $\epsilon=0$ (at the equilibrium), $\epsilon=0.1$ (at the stress peak) and $\epsilon=0.12$ (after the stress peak) in the atomic layers S_1, S_2, \dots perpendicular to the $[101]$ tensile direction. The (red) circles indicate the AIMD average positions of the atoms at each strain deformation step. For clarity, the atomic displacements relative to the average positions are enlarged by a factor of 3. (b) A $1 \times 1 \times 2$ cubic-supercell of Al that defines the S_1, S_2, \dots atomic layers perpendicular to the $[101]$ tensile direction. (c) The enlarged motion trajectory of an Al atom in the S_2 layer.

Fig. 4 (Color online) The calculated phonon spectra of Al in the Brillouin zone of a fcc

unit cell at temperatures $T=0$ (harmonic approximation), 300 and 700 K deformed along various tensile and shear directions at the strains after imaginary phonon frequencies appear at $T=0$ K. The imaginary frequencies are represented by the negative frequencies. The lattice vectors of the Al fcc unit cell at the equilibrium structure are $\vec{a}_1 = a(\vec{j} + \vec{k})/2$, $\vec{a}_2 = a(\vec{i} + \vec{k})/2$, and $\vec{a}_3 = a(\vec{i} + \vec{j})/2$, which will change under structural deformations. The k points in the phonon spectra are defined as $\Gamma = (0, 0, 0)$, $L = (0.5, 0.5, 0.5)$, $K = (0.625, 0.625, 0.25)$, $X = (0.5, 0.5, 0)$, $L' = (0.5, 0, 0)$, $K' = (0.625, 0, 0.375)$ and $X' = (0.5, 0, 0.5)$, in units of the reciprocal lattice vectors $\{\vec{b}_i\}$ associated with $\{\vec{a}_i\}$. The k points (L, K, X) and (L', K', X') become nonequivalent under structural deformations.

Figures

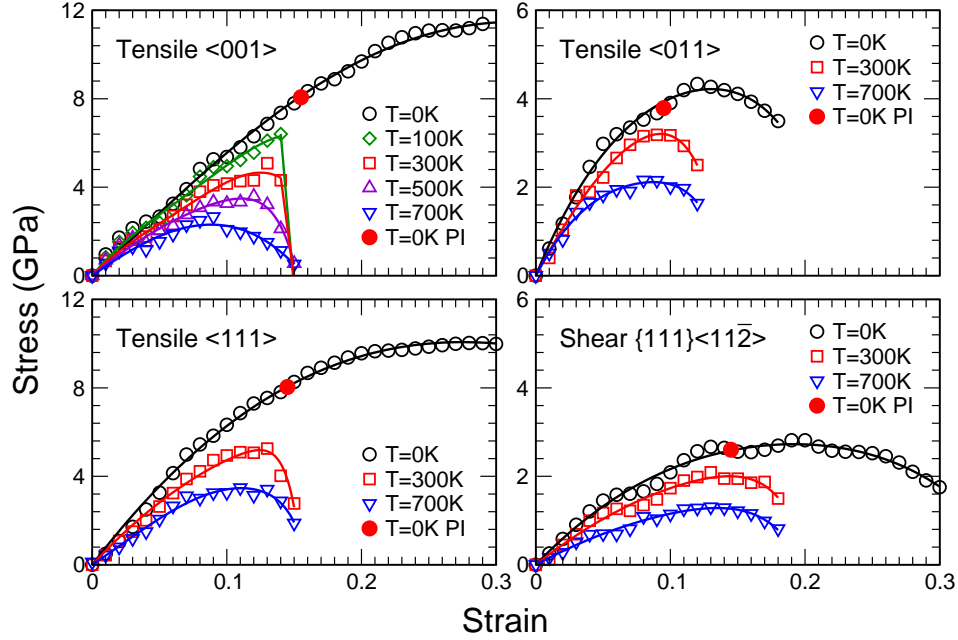


FIG. 1: (Color online) The AIMD calculated average stress-strain relations of Al in a cubic supercell with 32 Al atoms under various tensile and shear deformation directions at different temperatures. The (red) solid circles indicate the phonon instability (PI) determined at $T=0$ K, which begins at the strains equal to 0.155, 0.095, 0.145 and 0.145, respectively, for the $\langle 001 \rangle$, $\langle 011 \rangle$, $\langle 111 \rangle$ uniaxial tension and the $\{111\}\langle 11\bar{2} \rangle$ shear deformation.

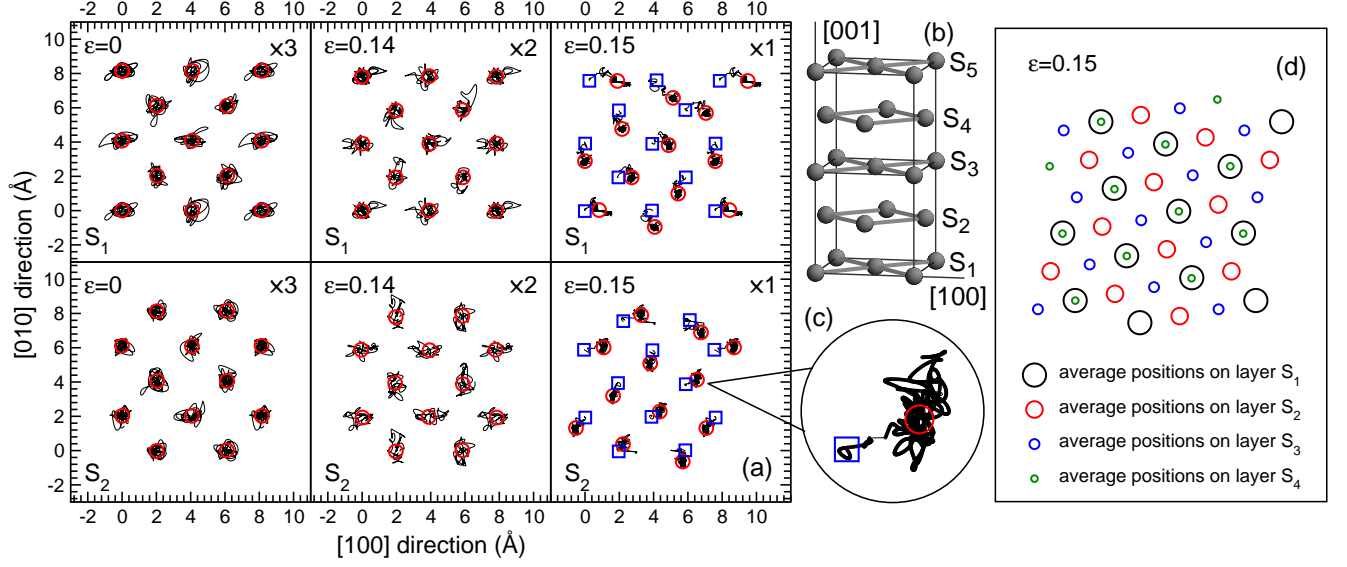


FIG. 2: (Color online) (a) The calculated AIMD motion trajectory (solid lines) of atoms in an Al $2 \times 2 \times 2$ cubic-supercell at $T=300$ K under the [001] tensile strains $\epsilon=0$ (at the equilibrium), $\epsilon=0.14$ (before the stress drop) and $\epsilon=0.15$ (just after the stress drop) in the atomic layers S_1, S_2, \dots perpendicular to the [001] tensile direction. The (blue) squares and (red) circles indicate the initial and AIMD average atomic positions at each strain deformation step. For clarity, the atomic displacements relative to the average positions are enlarged by a factor of 3 and 2 for $\epsilon = 0$ and 0.14, respectively. (b) A $1 \times 1 \times 2$ cubic-supercell of Al that defines the S_1, S_2, \dots atomic layers perpendicular to the [001] tensile direction. (c) The enlarged motion trajectory of an Al atom in the S_2 layer. (d) The calculated AIMD average atomic positions in the S_1, \dots, S_4 layers for a $2 \times 2 \times 6$ cubic-supercell at $T=300$ K and under the [001] tensile strain at $\epsilon = 0.15$.

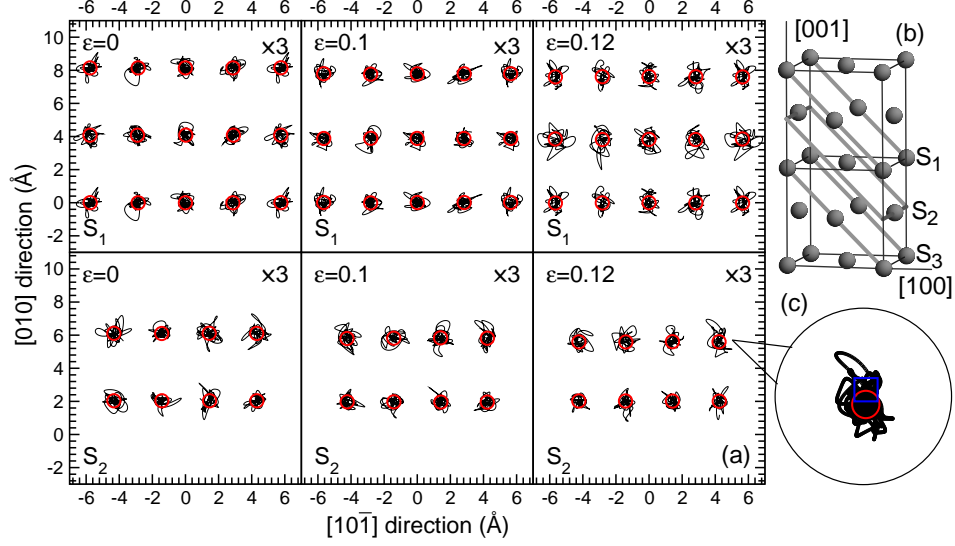


FIG. 3: (Color online) (a) The calculated AIMD motion trajectory (solid lines) of atoms in an Al $2 \times 2 \times 2$ cubic-supercell at $T=300$ K under the $[101]$ tensile strains $\epsilon=0$ (at the equilibrium), $\epsilon=0.1$ (at the stress peak) and $\epsilon=0.12$ (after the stress peak) in the atomic layers S_1, S_2, \dots perpendicular to the $[101]$ tensile direction. The (red) circles indicate the AIMD average positions of the atoms at each strain deformation step. For clarity, the atomic displacements relative to the average positions are enlarged by a factor of 3. (b) A $1 \times 1 \times 2$ cubic-supercell of Al that defines the S_1, S_2, \dots atomic layers perpendicular to the $[101]$ tensile direction. (c) The enlarged motion trajectory of an Al atom in the S_2 layer.

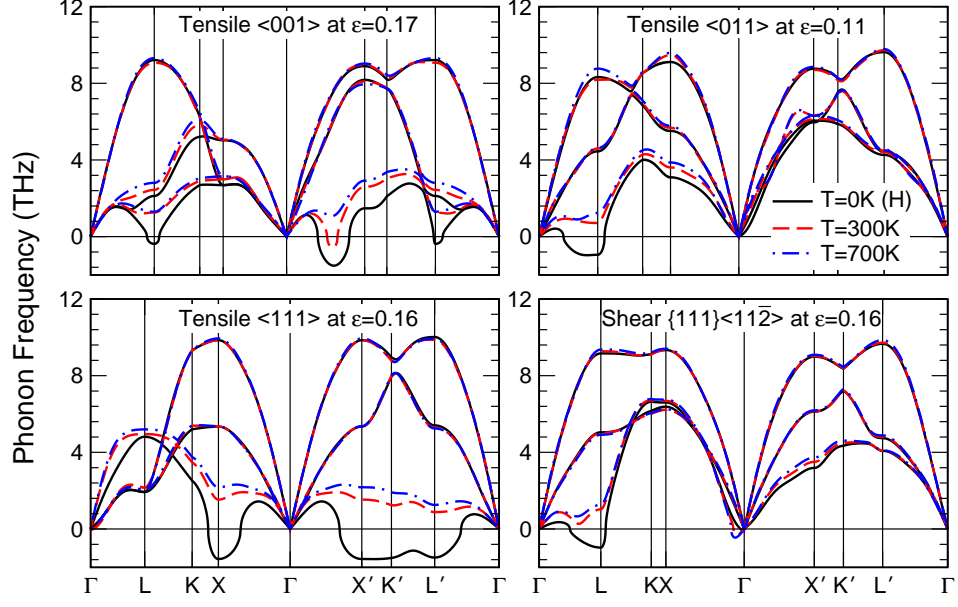


FIG. 4: (Color online) The calculated phonon spectra of Al in the Brillouin zone of a fcc unit cell at temperatures $T=0$ (harmonic approximation), 300 and 700 K deformed along various tensile and shear directions at the strains after imaginary phonon frequencies appear at $T=0$ K. The imaginary frequencies are represented by the negative frequencies. The lattice vectors of the Al fcc unit cell at the equilibrium structure are $\vec{a}_1 = a(\vec{j} + \vec{k})/2$, $\vec{a}_2 = a(\vec{i} + \vec{k})/2$, and $\vec{a}_3 = a(\vec{i} + \vec{j})/2$, which will change under structural deformations. The k points in the phonon spectra are defined as $\Gamma = (0, 0, 0)$, $L = (0.5, 0.5, 0.5)$, $K = (0.625, 0.625, 0.25)$, $X = (0.5, 0.5, 0)$, $L' = (0.5, 0, 0)$, $K' = (0.625, 0, 0.375)$ and $X' = (0.5, 0, 0.5)$, in units of the reciprocal lattice vectors $\{\vec{b}_i\}$ associated with $\{\vec{a}_i\}$. The k points (L, K, X) and (L', K', X') become nonequivalent under structural deformations.